Enhanced Conversion Efficiency Enabled by Species Migration in Direct Solar Energy Storage

Guanzhou Lin,^[a] Husain Almakrami,^[a] Huzaifa Emran,^[a] Amar Ruthen,^[b] Jie Hu,^[a] Zi Wei,^[a] Fuqiang Liu*^[a]

[a] G. Lin, H. Almakrami, H. Emran, J. Hu, Z. Wei, Prof. F. Liu* Department of Mechanical Engineering University of Massachusetts Lowell Lowell, Massachusetts 01854, USA Email: fuqiang_liu@uml.edu

[b] A. Ruthen Concord-Carlisle Regional High School 120 Meriam Rd Concord. MA 01742

Supporting information for this article is given via a link at the end of the document.

Abstract: Solar energy can be stored via either an indirect route in which electricity is involved as an intermediate step, or a direct route that utilizes photogenerated charge carriers for direct solar energy conversion. In this study, we investigate the fundamental difference between the direct and indirect routes in solar energy conversion using a new photoelectrochemical energy storage cell (PESC) as a model device. This PESC centers on a liquid junction that utilizes CH₃NH₃Pbl₃ perovskite to drive photoelectrochemical reactions of Benzoquinone (BQ) and Ferrocene (Fc) redox species. The experimental studies show that the equilibrium redox potentials are 0.1 V and -0.78 V (vs Ag/AgNO₃) for Fc⁺/Fc and BQ/BQ•-, respectively, which would produce a theoretical open-circuit voltage of 0.88 V for the storage device. The physicsbased computational analysis shows a relative flat reaction rate distribution in the electrode for the indirect route; however, in the direct route the photoelectrochemical reaction rate is critically affected by electron concentration due to strong light absorption of the perovskite material, which has been shown to vary by at least 10-fold in the transverse direction across the photoelectrode. The drastic variation of reaction rate in the photoelectrode creates an electric field that is 7.5 times stronger than the bulk electrolyte, which causes the photo-converting reaction product (i.e., BQ•-) to drift away from the photoelectrode thereby creates a constant reaction driving force. As a result, it has been shown that the intrinsic solar to chemical conversion (ISTC) efficiency has been improved by ~ 40% for the direct route compared to the indirect route at 0.05 mA/cm².

Introduction

Due to its intermittency, solar energy is often converted to chemical energy in energy carriers such as solar fuels and other energy-rich products, which can be stored for later use when sunlight is not available. This could substantially improve reliability, availability, and quality of the renewable energy source. Traditionally, these energy carriers are produced via an indirect route in which electricity is first produced in a solar cell, as an intermediate step, and is further used in an electrochemical device, either an electrolyzer or battery. Alternatively, a direct route relies on photoactive materials (e.g., semiconductors) and utilizes photogenerated electrons (high reducing power) and holes (oxidizing power) for direct solar energy conversion reactions.

Compared to the indirect route, the direct route has developed rapidly over the past decade. Many existing systems utilizing the direct route are based on two different approaches: 1) artificial

photosynthesis converting and storing solar energy into solar fuels; 2) direct solar energy storage through reversible redox reactions. The former is limited by a narrow choice of solar fuels, including hydrogen by photo-catalytic water splitting^[1, 2], ammonia by photocatalytic N₂ reduction^[3], or alcohols from CO₂ reduction^[4]. Though prior research has established efficient semiconductor structures^[5-10] and optimized photoelectrochemical (PEC) cells^{[11-} 13], artificial photosynthesis still suffers from low solar energy conversion efficiency due to a constrained thermodynamic driving force (determined by the band structure of semiconductors and chemical inertness of CO₂, N₂, and H₂O). The latter, however, could use redox reactions that are several orders of magnitude faster than those in artificial photosynthesis[14] and thus a higher solar energy conversion and storage efficiency could be achieved. A large number of existing studies in the broader literature have examined different systems that are also widely utilized in flow redox flow batteries, including vanadium species[15-^{21]}, quinone^[22, 23], zinc-iodine and bromine-iodine redox system^[24], and ferrocyanide[25].

The motivation behind the fast development of the direct route in solar energy storage is the common belief that the direct route can become more efficient as compared to its indirect counterpart because it directly utilizes the photogenerated charge carriers without intermediate energy conversion steps^[26]. Haussener et al[27] studied PEC water-splitting processes and showed that an integrated system (i.e., direct route) outperformed the conventional PV-electrolyzer system (indirect route). example, with the same light absorber tandem cell structure (Si/GaAs), the efficiencies for the integrated system and the conventional PV-electrolyzer system were 15.3% and 13.3%, respectively, with assumed electrolyzer efficiency of 75% and DC-DC-converter efficiency of 85%. Although it was postulated that the direct route benefits from a larger internal electrolyzer efficiency because of diminished overpotentials at small current densities, the key attributes pertaining to potentially higher efficiency of the direct route are not well understood in the literature. In part, this is because indirect and direct routes may have different operating current regimes and geometric parameters in non-ideal electrolytic systems.

In order to properly address the fundamental differences between the direct and indirect routes, in this work we first developed a new photoelectrochemical energy storage cell (PESC) using CH₃NH₃Pbl₃ (MAPbl₃) perovskite in combination with a Benzoquinone (BQ)-Ferrocene (Fc) redox system. We then performed both experimental and theoretical investigations on the developed PESC, as a model device, and compared with the indirect route that consisted of a solar cell and a redox flow

battery. Our results revealed that in a PESC a steep electric field in the electrode forces the reaction products to drift away from the reaction sites, and thus creates a constant reaction driving force to improve the intrinsic solar to chemical conversion (ISTC) efficiency. This discovery may guide us to ultimately exploit the benefits of the direct route and design efficient artificial photosynthetic systems.

Results and Discussion

Design of the photoelectrochemical energy storage cell.

The design of the PESC was inspired by a recent work from Bard's group at UT Austin who demonstrated a liquid-junction perovskite cell based on p-MAPbl₃ and achieved an open-circuit voltage (V_{oc}) of 1.05 V and a photocurrent density of 11 mA.cm⁻²

at 0.5 V bias voltage^[28]. In this work, we replaced the hole and electron transport layers (HTL and ETL) commonly used in conventional solar cells with two pairs of nonaqueous redox i.e., ferrocenium/ferrocene (Fc⁺/Fc) benzoquinone semiquinone/radical anion (BQ/BQ•-, "•" stands for the radical) in the developed PESC (Figure 1a) to extract holes and electrons from the perovskite photoelectrode (PE). Photovoltage was determined by the difference electrochemical potentials of the redox couples that were separated by a membrane (Figure 1b). Most importantly, the redox species were utilized as efficient energy media and solar energy could be directly converted/stored into chemical energy at the semiconductor-liquid electrolyte interface without the intermediate step such as electricity.

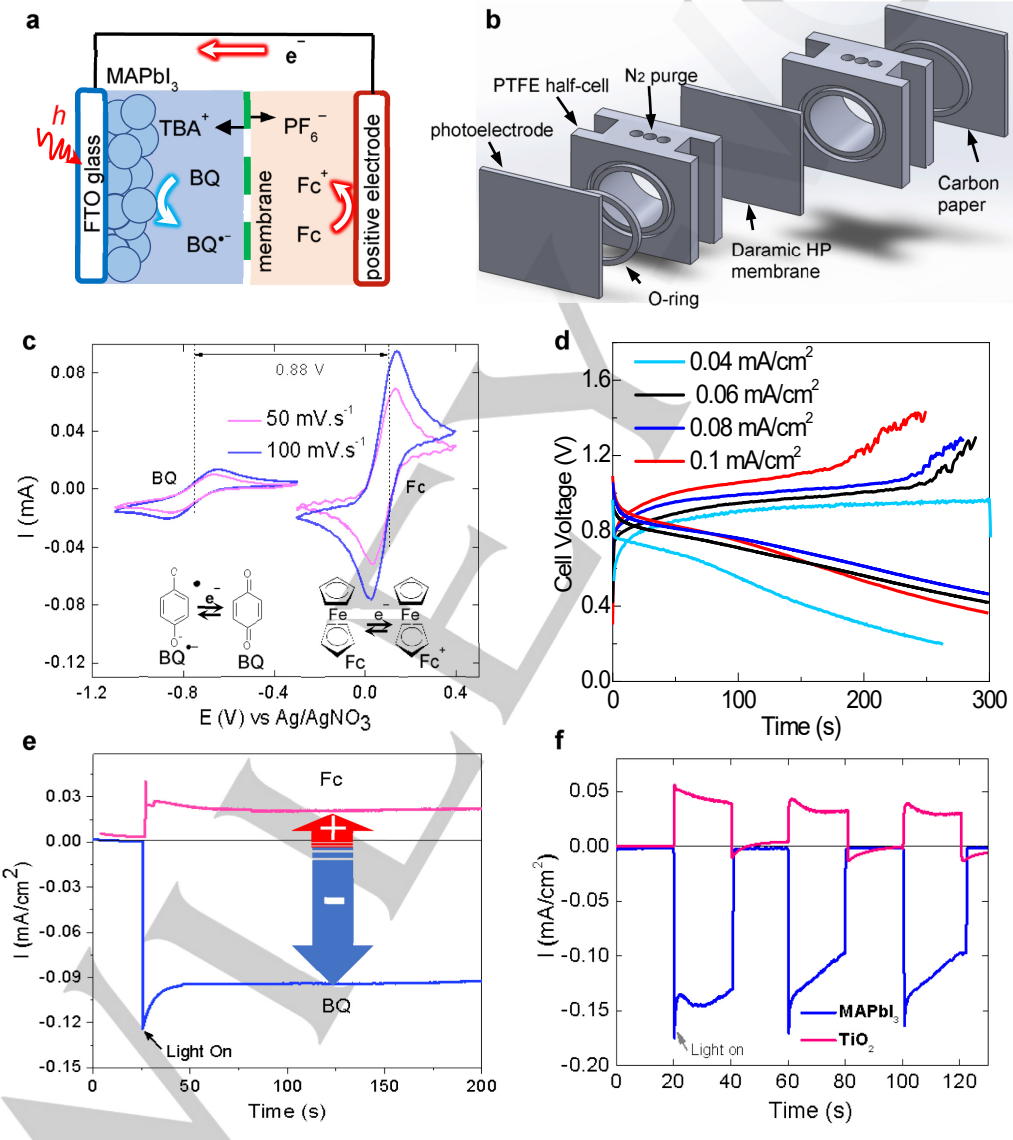


Figure 1. Electrochemical and photoelectrochemical characterization of the developed PESC. (A) Schematic illustration of the PESC setup. (B) Exploded view of the cell, including two PTFE half-cells, a membrane, electrodes, and electrolyte storage chambers. Charge extraction and solar energy storage are enabled by the respective reactions: $BQ + e^- \to BQ^-$ and $Fc \to Fc^+ + e^-$ at the photoelectrode (PE) and carbon paper counter electrode, respectively. (C) Cyclic voltammograms at variable scanning rates of 2 mM Fc in CH₃CN and 2 mM BQ in CH₂Cl₂. The working electrode is a glassy carbon and the supporting electrolyte is 0.1 M TBAPF₆. Open circuit voltage of the PESC was determined to be 0.88 V. (D) Charge-discharge curves of an RFB with 10 mL of 2 mM BQ/BQ^- and 2 mM Fc/Fc+. The cell was charged at different current densities (indicated in the figure) and discharged at 0.02 mA/cm². The supporting electrolyte is 0.1 M TBAPF₆. SGL carbon papers were used as the electrodes and the test was carried out at room temperature under continuous N₂ flow. (E) Zero-biased photocurrents under zero-resistance ammetry (ZRA) protocol in a three-electrode cell, in which a MAPbl₃ PE was in contact with either BQ or Fc. An Ag/AgNO₃ (0.01M in CH₃CN) electrode and a Pt mesh were used as the reference and counter electrodes, respectively. (F) Photocurrents of two PESCs, i.e., $TiO_2 | Fc | Daramic HP$ membrane | BQ | Counter electrode and MAPbl₃ | 2 mM BQ | Daramic HP membrane <math>| 2 mM Fc | Counter electrode and electrode and conditions.

Electrochemical characterization of redox species.

Electrochemical characterization of BQ and Fc was conducted in a three-electrode electrochemical cell. Figure 1c shows the cyclic voltammograms of BQ and Fc both at 2 mM balanced with 0.1 M TBAPF₆ in CH₂Cl₂ and CH₃CN, respectively. CH₂Cl₂ is a nonpolar solvent that was used to stabilize the perovskite photoelectrode. Well-defined oxidation (at 0.16 V vs. Ag/AgNO₃) and reduction peaks (at 0.03 V) of Fc+/Fc were observed with an anodic to cathodic peak current ratio close to unity. This indicates high reversibility of the one-electron electrochemical transfer process and also explains why this stable redox couple has been widely used in reference electrodes for nonaqueous electrolytes. Besides, the peak-to-peak separation yields a potential difference of 0.1 V at 50 mVs⁻¹, which slightly increases as the sweeping rate doubles. In contrast, the oxidation and reduction peaks of BQ are suppressed and largely separated suggesting a relatively slower electron transfer kinetics as shown in Figure 1c. The equilibrium redox potentials are determined to be 0.1 V and -0.78 V (vs $Ag/AgNO_3)$ for Fc^+/Fc and $BQ/BQ^{\bullet -},$ respectively, which would produce a theoretical open-circuit voltage of 0.88 V for the developed PESC.

A redox flow battery (RFB) was constructed according to Figure 1b with the PE replaced with an SGL carbon paper. Electrochemical cycling of the RFB was carried out under variable current densities as exhibited in Figure 1d. The cell was charged at different current densities and discharged at 0.02 mA/cm². The test was repeated in multiple cycles using 10 mL of 2 mM Fc and BQ electrolytes with continuously flowing N₂ to remove trace O₂ and moisture from the nonaqueous electrolytes. The cell reached the theoretical V_{oc} (0.88 V) at the charging current of 0.04 mA/cm² and a voltage of 0.2 V at the end of discharging cycles. Higher voltages were achieved as the charging current increased. This suggests that the cell approaches its full storage capacity towards the end of the charging cycles when higher charging currents are applied. In addition, similar discharge profiles but much higher discharge voltages are obtained when the charging current was between 0.06 - 0.1 mA/cm². The energy efficiency estimated from Figure 1d ranges from 32% to 60% as the rate decreases from 0.1 to 0.04 mA/cm². These achieved energy efficiencies, though suffered from losses due to large concentration polarization, are on a par with or higher than reported state-of-the-art nonaqueous RFBs in literatures[29].

Photoelectrochemical study of the PESC.

To further demonstrate the effectiveness of the BQ/BQ- and Fc⁺/Fc as charge transport agents in the PESC, we investigated whether the redox species, as either HTL or ETL, could efficiently transport the photogenerated charge carriers from the PE-liquid junction. We chose MAPbl₃ perovskite as the PE material owing to its decent band gap of 1.53 eV[28], high absorption coefficient[30] and outstanding electronic properties [31]. In a traditional threeelectrode electrochemical cell, an MAPbl₃ PE on FTO was immersed in either 2 mM BQ or Fc. Figure 1e shows that the polarity of charge transfer can be controlled using different redox species and the magnitude of the photocurrents is related to the nature of the PEC reactions. Using Fc results in a current flowing from the perovskite to the electrolyte, defined as positive, whereas BQ yields a negative photocurrent. Corroborated by MAPbl₃ perovskite's ambipolar carrier transport characteristics^[32] and its photoinduced self-doping mechanism via the formation of positively and negatively charged vacancies[33], migration of the vacancies in the electric field because of different redox species seems to be responsible for the appearance of either a P-type or N-type material. Our results clearly demonstrated that charge transfer at the perovskite/electrolyte interface can be directly modulated by the redox couples.

Furthermore, to verify the effectiveness of MAPbl $_3$ as a PE material, we compared its PEC performance with that of TiO $_2$. Two PESCs were constructed with the following different configurations: TiO $_2$ | 2 mM Fc | Daramic HP membrane | BQ |

counter electrode and MAPbl $_3$ | 2 mM BQ | Daramic HP membrane | 2 mM Fc | counter electrode, where the symbol "|" denotes a phase boundary. In this work, TiO $_2$ was exclusively used to assess the interplay between redox species and semiconductors in photocharging of the developed storage cell. The cell photoresponse in the alternate light and dark conditions is depicted in Figure 1f. In the first cycle, the TiO $_2$ PE generates a photocurrent of 0.055 mA/cm 2 which declines but stabilizes after several illumination-dark cycles. In contrast, the MAPbl $_3$ PE demonstrates a much higher photocurrent (0.14 mA/cm 2) in 2 mM BQ electrolyte. These results agree well with the energetic analysis (Supporting Information). However, the photocurrent slowly declines in subsequent illumination cycles that is attributed to the inevitable material degradation which is also responsible for the known photoinduced self-doping[33].

Computational analysis of charging processes of an RFB and PESC.

Our experimental results have collectively demonstrated the working principle and uniqueness of the developed PESC. To further elucidate the photocharging processes in the PESC and to identify the key differences between the conventional PV–electrolyzer system (via the indirect route) and the PESC (via the direct route) that could potentially contribute to a higher efficiency, we turned to multi-component physics-based models (detailed in the Supporting Information). Specifically, we developed two models corresponding to the two different charging routes. To facilitate a straightforward comparison between the two different types of solar energy storage routes, the two models were built on the same cell construction, shown in Figure S1, that closely resembles the experimental setup.

The PE thickness is an important parameter in determining the photocharging efficiency in the developed PESC. Ideally a porous PE could increase the reactive surface area, but it also weakens light absorption as the generated charge carrier concentration abruptly drops as light travels into the PE (Figure S2). Simulation results (see the "Photoelectrode Thickness Analysis" section in the Supporting Information) and Figure S3 also show that a porous PE renders more uniform utilization of the electrode but requires thicker electrodes for a complete absorption of the incident photons. Furthermore, Figure S4 and S5 and the related discussion (in the "Normalized Power Distribution and Photon Flux" section in the Supporting Information) suggest that a porous PE thinner than 10 μm may not be able to fully utilize the incident light; therefore, a 50-µm electrode with the same porosity (50%) was chosen for the PE in a PESC and the electrode in a RFB to facilitate a straightforward comparison.

Since the PESC and RFB only differ in the negative electrode, we thus primarily focused on species transport in the catholyte compartment. Figure 2 compares the distribution of BQ*concentration in the catholyte (in contact with the PE) at two current densities with the migration term (i.e., $\frac{z_l F}{RT} D_l C_l \nabla \phi_l$) either on or off. At 0.02 mA/cm², Figure 2a reveals that as the PEC reactions proceed, the BQ concentration gradually increases as a result of the reaction BQ + e⁻ → BQ•⁻, particularly at the PE/FTO interface, and gradually the concentration profiles shift into the bulk electrolyte. In Figure 2b, turning on the migration term further shifts the BQ* concentration profiles to the bulk electrolyte and pronouncedly reduces the concentration both in the PE and at the PE/FTO interface. Such changes are ascribed to BQ* transport due to migration which has been shown to have a substantial influence on species distribution in a redox flow battery^[34]. This effect is even more conspicuous when the simulation was conducted at 0.05 mA/cm². The BQ*- concentration increases substantially in the PE in Figure 3c but turning on the migration term in the simulation reduces the interfacial BQ - concentration at least by half, which again proves the important implication of migration to charged species transport. In addition, BQ*concentration in Figure 3d appears to reach a peak in the catholyte which could result from the competing effects of diffusion and migration in the region.

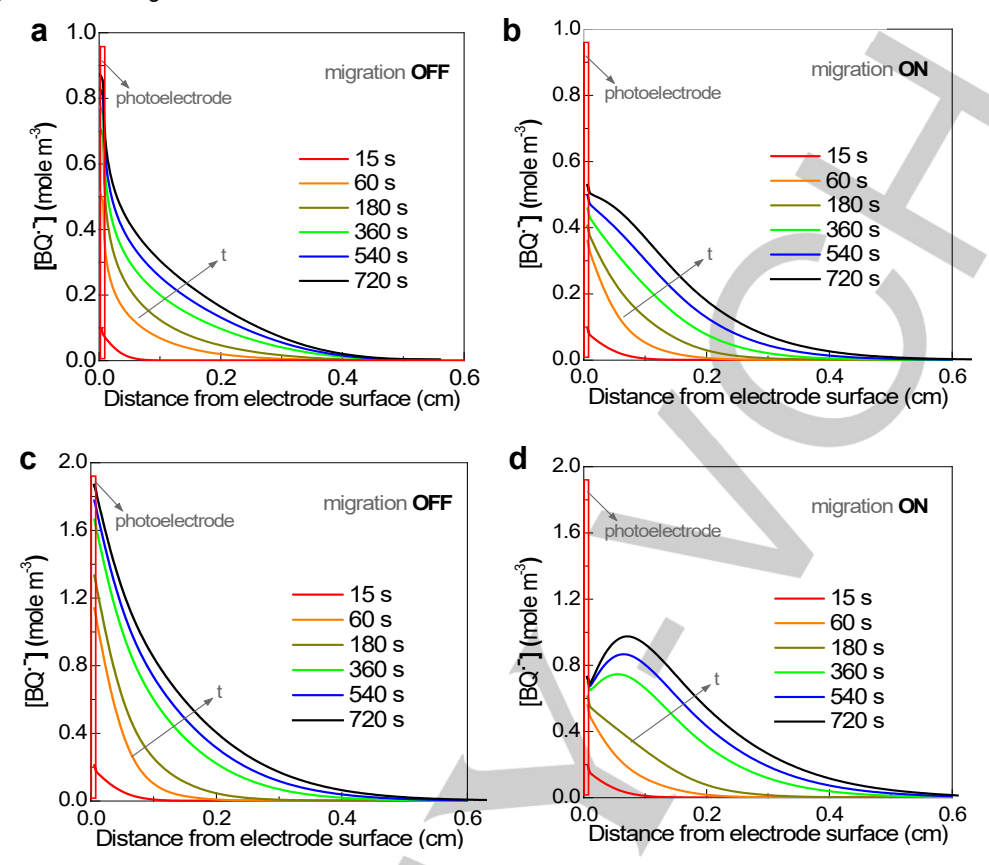
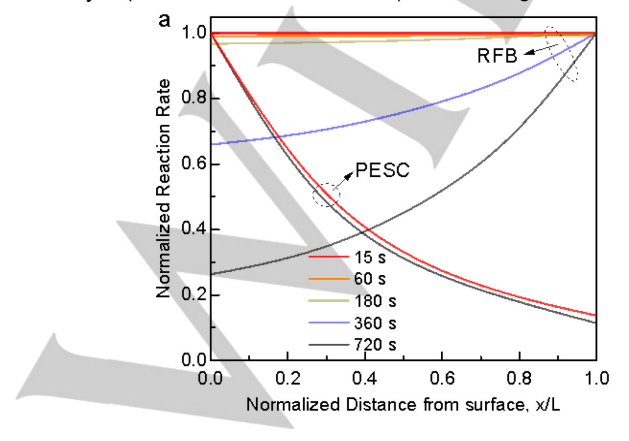


Figure 2. Transient BQ* concentration profiles in the catholyte of the PESC. (A)-(B) at 0.02 mA/cm² with (A) migration term turned off and (B) migration term turned on. (C)-(D) at 0.05 mA/cm² with (C) migration term turned off and (D) migration term turned on.

The above observation coincides strongly with the findings of Ju et al^[34]; however, the appearance of the peak BQ* concentration in the bulk catholyte rather than in the PE is unexpected. To further elucidate BQ* transport in the PE and catholyte, we first analyzed electrolyte potential distribution. In Figure S6, electrolyte potentials were plotted as a function of distance to the PE/FTO interface at 0.05 mA/cm² with and without migration. The electric field in the electrolyte, though slightly fluctuated for the case with migration, is directly related to the photocurrent and is not much affected by migration. In both cases, the strong electric field (estimated to be 13 V/m) in the PE and in the vicinity of the PE/electrolyte interface gradually diminishes to the value in the bulk electrolyte (estimated to be 1.73 V/m). The strong electric

field in the vicinity of the PE originates from the PEC generation of negatively charged BQ $^{\bullet}$ species which then enter the electrolyte and therefore significantly decrease the electrolyte potential in the vicinity of the PE. As a result, this strong electric field could drag a large amount of BQ $^{\bullet}$ species away from the PE to the adjacent electrolyte, where they are accumulated as the electric field is much diminished. Therefore, a concentration peak of BQ $^{\bullet}$ species emerged due to an imbalance between the BQ $^{\bullet}$ ingress rate from the PE and the egress rate from this region to the bulk electrolyte.



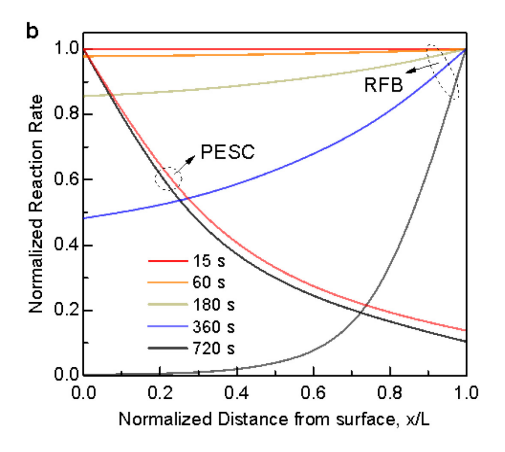


Figure 3. Normalized photo-/electrochemical reaction rate distribution in an RFB electrode and a PESC photoelectrode. (A) current density of 0.02 mA/cm² and (B) current density of 0.05 mA/cm². Both electrodes have the same thickness – 50 μ m. The interfaces x/L=0 and x/L=1.0 correspond to those of the current collector (or FTO)/electrode and electrode/electrolyte, respectively.

On the other hand, the impact of migration is insignificant in an RFB. As can be seen in Figure S7, migration only slightly reduces BQ - concentration near the negative electrode either at higher currents or after prolonged charging. These results are in sharp contrast to those in a PESC shown in Figure 2. We hypothesize that the different implication of migration to species transport in a PESC and an RFB may be attributed to different reaction rate distribution in their electrodes. The electrochemical reaction kinetics of an RFB is simply governed by Butler-Volmer equation (Eqs. S3 and S4 in the Supporting Information) and the reaction rate distribution in the electrode is controlled by both species concentration and overpotential. However, the former seems to be dominating under the low-current and low-speciesconcentration operating conditions in this study, resulting in a gradually declining reaction rate from the electrode/electrolyte interface (x/L=1) to the current collector/electrode interface (x/L=0) during charge. Figure 3a shows that electrochemical reaction rate is uniform at the beginning of charge; however, the electrode near the bulk electrolyte appears more reactive specially at high currents or near completion of charge. In the PE of a PESC, the PEC reaction rate (described by Eq. S20) is strongly affected by electron concentration, which has been shown to vary by at least one order of magnitude in the transverse direction across the PE (Figure S2), thus causing an abrupt change of reaction rate across the PE (Figure 3b). The distinct difference of reaction rate distribution in electrodes of an RFB and a PESC is especially important since the produced BQ* species and therefore the overall charge density will be vastly varied in them. In an RFB, more BQ*- species are produced at the interface where x/L=1 and therefore according to Poisson's equation a localized electric field that opposes the global electric field in the cell as shown in Figure S3 is created. In contrast, the strong localized electric field in the PE of a PESC, established due to a large charge density gradient, aligns with the global electric field in the cell as shown in supplementary Figure S3. This electric field is forcing the negatively charged species (BQ*- and PF6-) to drift away from the PE/FTO interface and therefore creating a "depletion region" that is analogous to the classic P-N junction formation in semiconductors.

Intrinsic solar to chemical conversion efficiency.

Because of different BQ* concentration profiles in a PESC and an RFB, different energy conversion scenarios emerge depending on the used electrode. When an MAPbl₃ PE is employed in a PESC, the dramatically reduced BQ* concentration in the "depleted" PE helps to maintain a fairly stable equilibrium potential of BQ/BQ*- ($E_{BQ/BQ}{\mbox{\tiny $^{\bullet}$-}}$) according to the Nernst equation (Eq. S7). As conspicuously manifested in Figure 4a, $E_{BO/BO}$ at the PE/electrode interface is about 0.2 V more positive than the conduction band (CB) edge of MAPbl₃. Note that the CB edge of MAPbl₃ is designated as - 0.7 V in the electrochemical scale as is typically reported in literatures[35-38]. Therefore, the photogenerated electrons in $MAPbl_3$ could be effectively extracted by the redox system because of their relative energy levels. Such a charge carrier transfer process is deemed favorable and stable because it has a constant driving force taken as the difference between the MAPbI3 CB edge and $E_{BQ/BQ^{\bullet-}}$ Most importantly, as BQ- species drift away from the PE, the back reaction of BQ • being oxidized by any surface holes, which resembles a "shorting circuiting" [39] path and is also equivalent to electron-hole recombination, is significantly minimized that may render a higher conversion efficiency.

However, in an RFB electrode (porous carbon paper), due to the negligible effect of migration BQ*-concentration rapidly builds up in the electrode, particularly at the current collector/electrode interface, which promptly raises the charging voltage as seen in both the experiments and simulation (Figure 4a). This is accompanied by fast declining $E_{BQ/BQ}$ *- and simultaneously rising E_{Fc} *-Fc*- as manifested in Figure 4a, which has substantial

implication to the intrinsic solar to chemical conversion (ISTC) efficiency^[40]. The ISTC efficiency is described by the following equation:

ISTC =
$$\frac{0.88}{E_{\text{Fc}^+/\text{Fc}^-}E_{\text{BQ/BQ}^{\bullet-}}} \times \frac{J_{\text{photo}} \times V_{\text{photo}}}{P_{\text{photo}}}$$
(1)

where 0.88 is the experimentally determined cell $V_{\rm oc}$, $E_{\rm Fc^+/Fc^-}$ $E_{\rm BO/BO}$ is the voltage across the cell and also the minimum charging voltage, $P_{\rm photo}$ is the incident illumination power density, and $J_{\rm photo}$ and $V_{\rm photo}$ are the photocurrent and photovoltage of the solar cell, respectively. Charging an RFB at J_{photo} = 0.2 mA/cm² and V_{photo} = 1.0 V caused an initial sudden drop of the ISTC efficiency followed by a gradual reduction over the course of the charging period (Figure 4b). Lowering the solar cell photovoltage from 1.0 V to 0.9 V reduced the ISTC efficiency by \sim 10%. In contrast, there was no change in ISTC efficiency for a PESC, which is supported by the established constant driving force (i.e., difference between the MAPbI $_3$ CB edge and $E_{BQ/BQ} - -$) for the photoelectron transfer reaction at the PE/electrolyte interface (Figure 4a). Figure 4b further illustrates the effects of varying charging current density from 0.02 to 0.05 mA/cm² on the ISTC efficiency. As the charging current density increases to 0.05 mA/cm², both the RFB and PESC improve their ISTC efficiency, but the change of the latter is more pronounced. In the entire charging period shown in Figure 4b, the ISTC efficiency of the PESC is at least 12% higher. Meanwhile, the time-dependent decay of the ISTC efficiency for the RFB at 0.05 mA/cm² is more severe and the penalty of declining ISTC efficiency due to a lower V_{photo} (from 1.0 to 0.9 V) is more substantial. In other words, an RFB, as in contrast to a PESC, is incapable of efficiently removing the electrochemical reaction products from its electrode, therefore suffers a greater concentration overpotential loss at a higher current density.

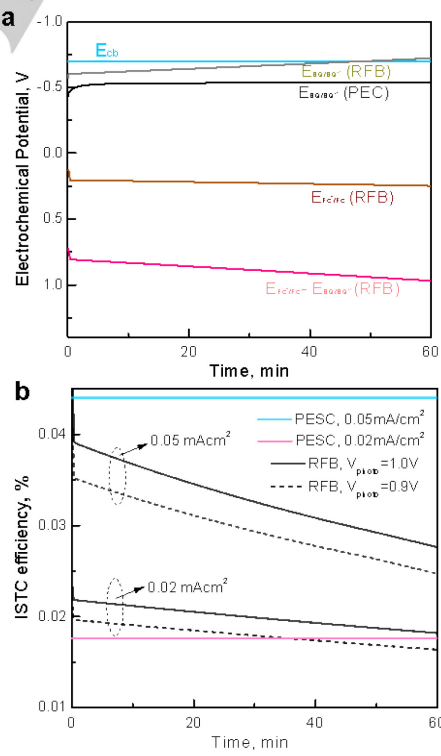
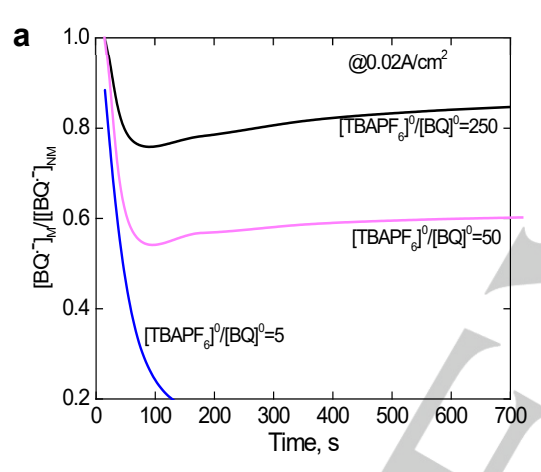


Figure 4. Transient electrochemical potentials and intrinsic solar to chemical conversion (ISTC) efficiency for an RFB and PESC during charge. (A) Electrode potentials at 0.2A/cm^2 as a function of charging time for both a RFB and PESC. The conduction edge potential, E_{cb} , is also labeled in the figure. (B) ISTC efficiency at two different charging currents.

Collectively, the data in Figures 3 and 4 demonstrates the advantage of a PESC in directly converting solar energy into chemical energy. This is due to the induced steep electric field in the PE that causes the negatively charged PEC products to drift

FULL PAPER

away, and therefore creates a constant reaction driving force and also a higher efficiency. However, the migration of BQ*- may be affected by the presence of foreign anions such as PF6 in the supporting electrolyte, which may compete with BQ*-. To test the above hypothesis, we conducted photocharging simulation with different supporting electrolyte TBAPF₆ concentrations, i.e., 0.01 M, 0.1 M, and 0.5 M. As expected, simulation results in Figures S8 and S9 showed that all charged species, including BQ-, TBA+, and PF₆-, migrate either from the PE to the bulk electrolyte, or the other way around, depending on their carried charges. This creates a PF₆ lean layer as well as a TBA+ rich layer near the electrode surface. Additionally, migration of BQ* from the PE surface seems to be weakened by high supporting electrolyte concentrations as judged by the steadily increasing surface concentration of BQ* (Figure S8 a, d, and g). However, a low supporting electrolyte concentration (e.g., 0.01 M) results in high resistance and simulation crashed after 180 s as shown in Figure S8a. On the other hand, increasing the photocurrent from 0.02 mA/cm² to 0.05 mA/cm² (Figure S9) not only causes much larger PF₆⁻ and TBA⁺ fluctuation in the electrolyte, but also results in a more effective reduction of surface concentration of BQ*-.



To further substantiate the above findings and quantify the effect of suppression of BQ* concentration, we investigated the ratios of BQ - concentration at the PE/FTO interface ([BQ -]M) to the counterpart without migration ([BQ*]_{NM}) at different charging currents and time. In Figure 5, quick reduction of BQ -concentration was found to occur within the beginning 50 s, followed by an almost stabilized [BQ•-]_M/[BQ•-]_{NM} value for the rest of the charging period. Additionally, a lower ratio of the supporting electrolyte (TBAPF₆) concentration to the initial BQ concentration, i.e., [TBAPF₆]⁰/[BQ]⁰, is more efficient in suppressing surface concentration of BQ*-, though instability may arise if the supporting electrolyte concentration was too low. On the other hand, though high [TBAPF₆]⁰/[BQ]⁰ ratios are ineffective in suppressing BQ*- concentration, it can be compensated by a high photocharging current. As seen in Figure 5 the stabilized [BQ*]_M/[BQ•-]_{NM} values reduced from 0.81 to 0.73 [TBAPF₆]⁰/[BQ]⁰=250 when the current increases from 0.02 to 0.05 A/cm², and more pronouncedly from 0.6 to 0.41 at [TBAPF₆]⁰/[BQ]⁰=50. Thus, the [TBAPF₆]⁰/[BQ]⁰ ratio closely correlates with the cell current density in suppressing surface BQ* concentration.

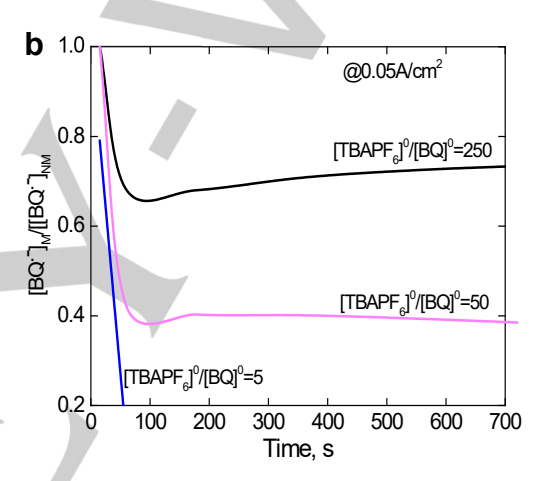


Figure 5. BQ $^-$ concentration ratio at the photoelectrode/FTO interface between the cases with migration ([BQ $^-$]_M) and without migration ([BQ $^-$]_{NM}). (A) at 0.02 A/cm². (B) at 0.05 A/cm². Different ratios of supporting electrolyte (TBAPF₆) concentration to initial BQ concentration ([TBAPF₆] 0 /[BQ] 0) are labeled in the figures.

Though in this work both experimental and computational studies have been primarily focused on small-current photocharge of the PESCs, the results shown in Figure 5 clearly demonstrate the correlative interactions between the supporting electrolyte concentration and photocharging current, which could provide insightful guidance for the design of high-current devices to directly harness solar energy.

Conclusion

In conclusion, in a PESC for direct conversion of solar energy a steep electric field in the photoelectrode could effectively force the reaction products to drift away, and create a constant reaction driving force to improve the solar energy conversion efficiency. Though what has been exemplified here employed an MAPbl₃ photoelectrode at low-current operating conditions, it is envisioned that the conclusions could be extended to different photoelectrode materials, as both photoanode and cathode, with different redox species and operating currents, as long as the supporting electrolyte concentration and operating current can be controlled to enable efficient migration of charged reaction products from the electrodes.

Experimental Section

Photoelectrochemical Energy Storage Cell

The schematic of the solar energy storage cell is illustrated in Figure 1b. The cell consists of an MAPbl₃ photocathode, a counter electrode, and two redox species, i.e., Fc⁺/Fc and BQ/BQ⁻, separated by a Daramic HP porous membrane (Daramic LLC, USA). The membrane was used to isolate the negative and positive compartments while allowing for charge transport of balancing ions (TBA⁺ and PF₆⁻) to complete the electrical circuit. The concentrations of BQ and Fc electrolytes were 2 mM in dichloromethane (DCM, CH₂Cl₂) and (CH₃CN), respectively, balanced with 0.1 M Tetrabutylammonium hexafluoro-phosphate (TBAPF₆) (Sigma-Aldrich).

Photoelectrode Fabrication

The MAPbl $_3$ photoelectrode was fabricated using a solution process according to references $^{[28,41]}$. In brief, equal moles of Pbl $_2$ (Sigma-Aldrich) and CH $_3$ NH $_3$ I (MAI) (Sigma-Aldrich) were mixed in dimethylformamide (DMF) (Sigma Aldrich) at ambient conditions. The prepared solution was stirred at 800 rpm and 80 °C for 15 min followed by spin-coating onto either a pre-cleaned FTO glass at 3000 rpm for 50 sec. The procedure was repeated three times to assure adequate film structure and to improve the film stability. Perovskite-coated films were then annealed at 100 °C on a hot plate for 20 min. The above procedures were conducted in a N $_2$ -filled glove box.

Electrochemical and Photoelectrochemical studies

FULL PAPER

Electrochemical characteristics of Fc⁺/Fc and BQ•-/BQ redox species were investigated by cyclic voltammetry (CV) using a three-electrode electrochemical cell and a potentiostat (Versa Stat 3, Princeton Applied Research) at scanning rates of 50 mV.s⁻¹ and 100 mV.s⁻¹. The three-electrode cell consisted of a glassy carbon (GC) working electrode (WE) (diameter = 3 mm), a Pt counter electrode (CE), and an Ag/AgNO₃ reference electrode (RE) (silver wire in 0.01M AgNO₃ dissolved in CH₃CN)^[28]. Electrochemical cycling studies were carried out using two carbon-paper electrodes (SGL, AA30) with continuous N₂ flow to remove trace oxygen from the electrolytes. Photoelectrochemical studies were conducted under AM1.5 condition using a solar simulator (Newport, 150 W Ozone free Xe lamp). Chronoamperometry measurements during photo-charge were conducted with no external bias voltage.

Multi-component Physics-based Models

Multi-component computational models were developed to understand charging processes in RFBs. These models were based on the experimentally validated electrochemical transport model^[42] developed for flow batteries. Transport of species in the electrolyte and the membrane separator was simulated according to the Nernst-Planck equation. Species generation and consumption due to photo-/electrochemical reactions were incorporated into the model as source terms. The electrochemical kinetics was formulated in the Butler-Volmer form and the photoelectrochemical reactions were formulated by a first-order kinetics with respect to the density of surface charges and reactants in the electrolyte. The two models were detailed in the "Electrochemical and Photoelectrochemical Models" section in the Supporting Information. Charge generation rate in perovskite photoelectrodes and charge-recombination kinetics were also included in the Supporting Information.

Acknowledgements

This work was funded by U.S. Natural Science Foundation (IIP-1918979).

Keywords: Solar Energy Storage • Perovskite • Species Migration • Redox species • Direct conversion

- [1] A. Fujishima, K. Honda, Nature. 1972, 238, 37-38.
- [2] P. Varadhan, H.-C. Fu, Y.-C. Kao, R.-H. Horng, J.-H. He, *Nat. Commun.* 2019, 10, 5282.
- [3] J. Zheng, Y. Lyu, M. Qiao, R. Wang, Y. Zhou, H. Li, C. Chen, Y. Li, H. Zhou, S. P. Jiang, S. Wang, Chem. 2019, 5, 617-633.
- [4] S. W. Sheehan, E. R. Cave, K. P. Kuhl, N. Flanders, A. L. Smeigh, D. T. Co, Chem. 2017, 3, 3-7.
- [5] K.-H. Ye, H. Li, D. Huang, S. Xiao, W. Qiu, M. Li, Y. Hu, W. Mai, H. Ji, S. Yang, *Nat. Commun.* **2019**, *10*, 3687.
- [6] Z. Zhang, I. Karimata, H. Nagashima, S. Muto, K. Ohara, K. Sugimoto, T. Tachikawa, *Nat. Commun.* 2019, 10, 4832.
- [7] B. Yao, J. Zhang, X. Fan, J. He, Y. Li Small. 2019, 15, 1803746.
- [8] Y. Li, Y. Xia, K. Liu, K. Ye, Q. Wang, S. Zhang, Y. Huang, H. Liu, ACS Appl. Mater. Interfaces. 2020, 12, 25494-25502.
- [9] K. Li, X. Lu, Y. Zhang, K. Liu, Y. Huang, H. Liu, *Environ. Res.* 2020, 185, 109409.
- [10] Y. Huang, Z. Guo, H. Liu, S. Zhang, P. Wang, J. Lu, Y. Tong, Adv. Funct. Mater. 2019, 29, 1903490.

- [11] P. Varadhan, H.-C. Fu, Y.-C. Kao, R.-H. Horng, J.-H. He, *Nat. Commun.* 2019, 10, 5282.
- [12] J. M. Yu, J. Lee, Y. S. Kim, J. Song, J. Oh, S. M. Lee, M. Jeong, Y. Kim, J. H. Kwak, S. Cho, C. Yang, J.-W. Jang, *Nat. Commun.* 2020, 11, 5509.
- [13] E. Kalamaras, M. Belekoukia, J. Z. Y. Tan, J. Xuan, M. M. Maroto-Valer, John M. Andresen, *Faraday Discuss.* 2019, 215, 329-344.
- [14] D. Liu, F. Liu, J. Liu, J. Power Sources. 2012, 213, 78-82.
- [15] Z. Wei, Y. Shen, D. Liu, F. Liu, Sci. Rep. 2017, 7, 629.
- [16] Y. Shen, Z. Wei, D. Liu, H. Almakrami, F. Liu, *Mater. Res. Bull.* 2017, 96, 431-436.
- [17] Z. Wei, Y. Shen, D. Liu, C. Hsu, S. D. Sajjad, K. Rajeshwar, F. Liu, *Nano Energy*. **2016**, 26, 200-207.
- [18] D. Liu, W. Zi, S. D. Sajjad, C. Hsu, Y. Shen, M. Wei, F. Liu, ACS Catal. 2015, 5, 2632-2639.
- [19] D. Liu, Z. Wei, Y. Shen, S. D. Sajjad, Y. Hao, F. Liu, J. Mater. Chem. A 2015, 3, 20322-20329.
- [20] Z. Wei, D. Liu, C. Hsu, F. Liu, Electrochem. Commun. 2014, 45, 79-82.
- [21] J. Azevedo, T. Seipp, J. Burfeind, C. Sousa, A. Bentien, J. P. Araújo, A. Mendes, Nano Energy. 2016, 22, 396-405.
- [22] Z. Wei, H. Almakrami, G. Lin, E. Agar, F. Liu, *Electrochim. Acta*.
- [23] W. Li, H.-C. Fu, L. Li, M. Cabán-Acevedo, J.-H. He, S. Jin, Angew. Chem. Int. Ed. 2016, 55, 13104-13108.
- [24] Y. Zhou, S. Zhang, Y. Ding, L. Zhang, C. Zhang, X. Zhang, Y. Zhao, G. Yu, Adv. Mater. 2018, 30, 1802294.
- [25] K. Wedege, J. Azevedo, A. Khataee, A. Bentien, A. Mendes, Angew. Chem. Int. Ed. 2016, 55, 7142-7147.
- [26] S. Styring Faraday Discuss. 2012, 155, 357-376.
- [27] S. Haussener, S. Hu, C. Xiang, A. Z. Weber, N. S. Lewis, *Energy Environ. Sci.* 2013, 6, 3605-3618.
- [28] H.-Y. Hsu, L. Ji, H. S. Ahn, J. Zhao, E. T. Yu, A. J. Bard, J. Am. Chem. Soc. 2015, 137, 14758-14764.
- [29] S.-H. Shin, S.-H. Yun, S.-H. Moon, RSC Adv. 2013, 3, 9095-9116
- [30] G. C. Papavassiliou, Mol. Cryst. Liq. Cryst. Sci. Technol., Sect. A 1996, 286, 231-238.
- [31] K. Yamada, H. Kawaguchi, T. Matsui, T. Okuda, S. Ichiba, *Bull. Chem. Soc. Jpn.* 1990, 63, 2521-2525.
- [32] F. Li, C. Ma, H. Wang, W. Hu, W. Yu, A. D. Sheikh, T. Wu, Nat. Commun. 2015, 6, 8238.
- [33] L. A. Frolova, N. N. Dremova, P. A. Troshin, Chem. Commun. 2015, 51, 14917-14920.
- [34] K. Oh, S. Won, H. Ju, Electrochim. Acta. 2015, 181, 238-247.
- [35] M. A. Green, A. Ho-Baillie, H. J. Snaith, Nat. Photonics. 2014, 8, 506-514.
- [36] L. Wang, G.-R. Li, Q. Zhao, X.-P. Gao, Energy Storage Mater. 2017, 7, 40-47.
- [37] I. Hussain, H. P. Tran, J. Jaksik, J. Moore, N. Islam, M. J. Uddin, Emergent Mater.. 2018, 1, 133-154.
- [38] S. Adjokatse, H.-H. Fang, M. A. Loi, *Mater. Today.* 2017, 20, 413-424.
- [39] A. J. Bard Journal of Photochemistry. 1979, 10, 59-75.
- [40] H. Dotan, N. Mathews, T. Hisatomi, M. Grätzel, A. Rothschild, J. Phys. Chem. Lett. 2014, 5, 3330-3334.
- [41] Y. Zhao, K. Zhu, J. Phys. Chem. C. 2014, 118, 9412-9418.
- [42] Z. Wei, N. A. Siddique, D. Liu, S. Sakri, F. Liu, Adv. Energy Res. 2016, 4, 285–297.

